CIGS P1, P2, and P3 scribing processes using a pulse programmable industrial fiber laser

Rekow, M.; Murison, R.; Dunsky, C.; Dinkel, C.; Pern, J.; Mansfield, L.; Panarello, T.; Nikumb, S.

Publisher's version / Version de l'éditeur:

Proceedings of the 25th EU PVSEC/WCPEC-5, pp. 3372-3374, 2010-09-10

CIGS P1, P2, P3 Scribing Processes using a Pulse Programmable Industrial Fiber Laser

M. Rekow[1], R. Murison[1], C. Dunsky[2], C. Dinkel[3], J. Pern[4], L. Mansfield[4], T. Panarello[1], and S. Nikumb[3]

[1]PyroPhotonics Lasers, Inc. 275 Rue Kesmark, Dollard-des-Ormeaux, Québec H9B 3J1, Canada
[2]Aeos Consulting, Inc. 72 Broadway, Los Gatos, CA 95030, USA
[3]NRC Canada, Industrial Materials Institute-CAMM, 800 Collip Circle, London, Ontario NG6 4X8 Canada
[4]National Center for Photovoltaics, National Renewable Energy Laboratory, 1617 Cole Boulevard, Golden, CO 80401, USA

ABSTRACT: We describe a novel set of laser processes for the CIGS P1, P2 and P3 scribing steps, the development of which has been enabled by a unique pulse-programmable fiber laser. We find that the unique pulse control properties of this 1064 nm wavelength laser have significant effects on the material removal dynamics of the various film layers in the CIGS material system. In the case of the P2 and P3 processes, the shaped pulses create new laser/material interaction effects that permit the material to be cleanly and precisely removed with zero Heat Affected Zone (HAZ) at the edges of the scribe. The new P2 and P3 processes we describe demonstrate the first use of infrared nanosecond laser pulses that eliminate the HAZ and the consequent localized compositional changes in the CIGS absorber material that result in poor shunt resistance. SEM micrographs and EDX compositional scans are presented. For the P1 scribe, we process the bi-layer molybdenum from the film side as well as through the glass substrate. Microscopic inspection and compositional analysis of the scribe lines are not sufficient to determine electrical and optical performance in working PV modules. Therefore, to demonstrate the applicability of the infrared pulse-programmable laser to all three scribing processes for thin-film CIGS, we fabricate small-size multiple-cell monolithically interconnected mini-modules in partnership with the National Renewable Energy Laboratory (Golden, Colorado). A total of four mini-modules are produced, two utilizing all laser scribing, and two with the P2 and P3 steps mechanically scribed (by a third party) for reference. Mini-module performance data measured at NREL is presented, and we also discuss the commercialization potential of the new single-laser CIGS scribing process. Finally we present a phenomenological model to describe this physics underlying this novel ablation process.
Keywords: CIGS, Thin Film Solar Cell, Laser Scribing, P2, P3

1 Background

CIGS is rapidly gaining ground as preferred material system for thin-film photovoltaics (PV). Among other advantages commercial CIGS PV modules can boast 13% [1] or more efficiency, are relatively non-toxic and environmentally benign, and have a very stable performance over time and environmental exposure. Given that the laboratory world record for CIGS efficiency is now 20.1% [2] the future for CIGS looks bright. Amid these obvious advantages, until now CIGS-based thin film PV modules have defied the traditional so-called P2 and P3 laser scribing processes [3] that have proven so valuable in creating the monolithic series interconnect structures required to achieve useful working voltage and current in large scale thin-film amorphous silicon and CdTe PV modules. With the failure of laser based processes, mechanical scribing with a force-controlled stylus has become the method of choice. This method can suffer, however, from poor edge quality (e.g., delamination, chipping, and variations over time due to mechanical wear). More importantly, the non-deterministic nature of the material removal mechanism yields wide, irregular scribe lines that necessitate large spacing between adjacent scribes. As a result, the CIGS modules suffer decreased efficiency [4]. Clearly a viable laser process would provide a tangible benefit to the mass production of CIGS thin film PV.

In addition to the P2 and P3 scribe processes, CIGS modules also require a P1 process. While there is a generally accepted laser process for the CIGS P1 scribe that utilizes 1064 nm wavelength and nanosecond pulses, until now the lasers used have proven completely ineffective for the P2 and P3 scribes.

In this paper we first describe a novel set of laser processes for the CIGS P1, P2 and P3 scribing steps, the development of which has been enabled by a unique pulse-programmable fiber laser [5]. Secondly we document the construction and test of monolithically integrated mini-modules utilizing these processes. Finally we present a simple phenomenological model that describes the physics of this novel ablation process and discuss the commercialization potential of these processes.

2 Scribe Process

Thin film solar cell laser scribing processes allow division of large solar modules into an array of smaller series interconnected cells on one monolithic substrate. These processes are integral to the cell fabrication process and must be performed at specific points in the manufacturing process to successfully form the monolithic series interconnected end product [3]. In a typical CIGS process, a laser is used to segment the first conductive layer (P1), typically Molybdenum (Mo), into adjacent, electrically isolated strips (or bands). Next, the CIGS absorber, CdS, and intrinsic ZnO (iZO) layers are deposited and in the P2 step, scribed down to the first conductive layer (Mo) with a slight offset from the underlying P1 scribe. Finally, another transparent conductive layer is added and scribed again (P3) with an offset from the previous P2 scribe. The area between the P1 and the P3 scribe becomes effectively inactive for the

purpose of generating electricity, and minimizing this so called "dead zone" is a primary motivation to consider a laser tool over a mechanical scribe tool. It should be noted that while it is only necessary to scribe the top conductive layer to make the P3 scribe, in practice the P3 scribe is made down to the bottom conductor layer (Mo) making it nearly identical to the P2 scribe.

2.1 Laser Source

The laser ultilized for this work was the 1064 nm PyroFlex™-25 pulse programmable fiber laser from PyroPhotonics [5]. This innovative new laser technology allows pulse duration to be varied from approximately 2 to several 100s of nanoseconds, independent of the laser repetition rate, which can be varied up to 500 kHz. In addition, each pulse can be arbitrarily programmed to generate a specific desired temporal profile of instantaneous laser power. Pulse trains comprised of these shaped pulses can be applied to the scribing process at high repetition rates. The same laser source and delivery optics was used to make all scribes. All process developement work and metrology was performed at NRC in London, Ontario and process development samples were provided by the National Renewable Energy Laboratory in Golden, Colorado.

2.2 P1 Process

The P1 process is generally considered a known process and many groups have reported successful and robust scribing processes utilizing Q-switched 1064nm lasers [6,7]. However it was discovered that the particular and unique bilayer structure employed at NREL for Molybdenum deposition process [8] resisted successful processing with previously published approaches. As a result substantial effort was invested in both glass-side and film-side process development.

In our experimental setup, the laser beam was expanded to the desired diameter, passed through a conventional variable attenuator device, and brought to focus on the test panel surface by a 100mm focal length lens. The sample was mounted on a 2-D linear scanning table to allow the laser beam to traverse its surface at variable speed. The scanning table was capable of reaching speeds of 800mm/s over a distance of ~6 inches. The lens was mounted on a vertical motion stage to enable rapid characterization of the depth-of-focus of the scribing process. The same basic configuration was utilized for all three (P1,P2, and P3) scribes.

For film side laser processing it was found that under no conditions could a single-pulse process remove the entire film cleanly. However it was determined that the first layer of this bilayer Mo structure could easily and cleanly be removed with a single 15µJ square-shaped 10ns pulse as illustrated in Figure 1-left. However, increasing the pulse energy invariably caused eruption of the underlying layer leaving a high protruding ridge as shown in Figure 1-right.

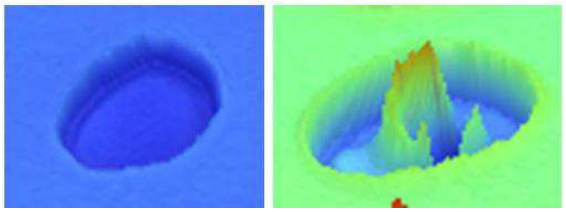

Figure 1: Wyko interferometric images of ablation in bilayer Molybdenum. Left: Clean ablation of the top Mo layer only, by a single laser pulse. Right: Clean ablation of top Mo layer with "eruption" of bottom Mo layer.

It was observed that the top layer was removed in its solid form by some sort of brittle fracture mechanism driven by rapid stress build up, while the bottom layer would soften due to heating, releasing the residual built-up stress. For the bottom layer, the driving forces apparently switched from stress build-up to phase transition and gas pressure accumulation, with resulting plastic deformation and rupture. Based on these observations, we hypothesized that creating a double pulse shape with a pair of 15µJ, 10ns square pulses separated by a 275ns delay would permit sufficient cooling of the bottom layer between the pulses so that the stress build-up mechanism would again become dominant by the time the second pulse impinged. The result was clean brittle removal of both top and underlying layers. Figure 2 shows the resulting film side P1 groove and illustrates the laser double pulse configuration that achieved these results. More details of this process are given in another publication [9].

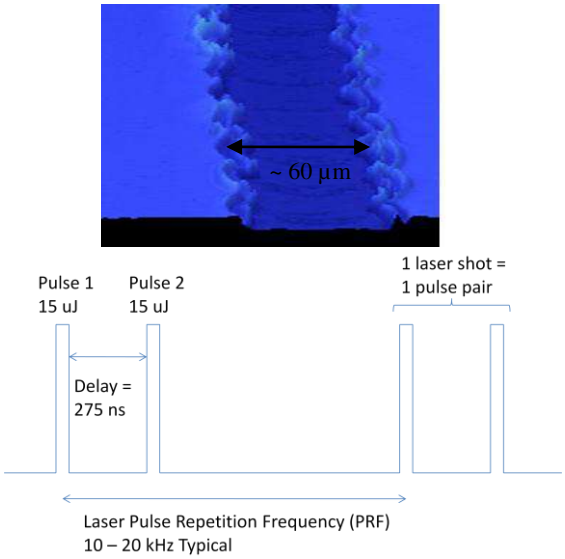

Figure 2: CIGS P1 film side process result utilizing a train of double pulses. Pulse 1 removes the first Mo layer and pulse 2 removes the second. The pulse pairs repeat at the trigger rate of the laser (PRF) and the trigger rate is set according to the sample motion speed such that adjacent laser "spots" have a slight overlap (30% typical) and form a continuous scribe line.

Development of a substrate-side (glass-side) process for this film presented different challenges. Initial results on a small sample look very good using single square 10ns, 50µJ pulses, however processing larger samples revealed that the process often failed on large areas of the film. Further study revealed that there was a correlation between the orientation of cracks on the Mo film surface and the onset of failure of the process, as shown in Figure 3. We speculate that the cracks indicate that the stress state of the film strongly influences the ablation process.

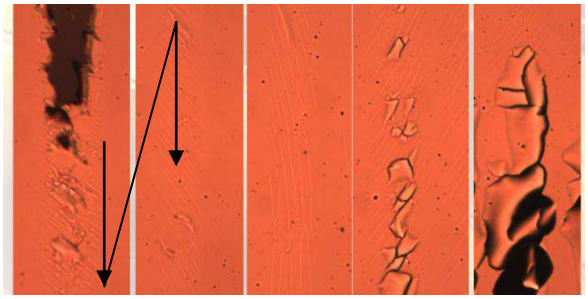

Figure 3: Orientation of crack pattern in area where initial P1 substrate-side ablation process failed. When crack pattern runs perpendicular to the scribe line the process begins to work. Where cracks have other orientations the ablation process fails.

We utilized the broad tunability of the PyroFlex™-25 laser to survey the pulse parameter space in order to find a regime where the stress state of the film did not spoil the ablation process. To do this we first ran an experimental matrix of spot size versus energy and selected the most promising parameter zone. Next, the pulse duration was optimized and it was found that there was a very narrow window from about 8 to 12 ns over which the process produced a clean scribe using square pulses (Figure 4). Once again, the ablation mechanism was observed to be that of a brittle fracture.

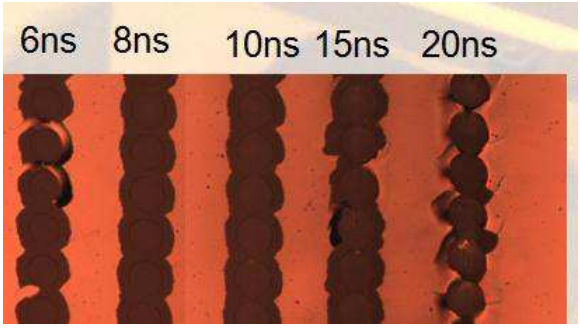

Figure 4: Ablation process behavior as a function of pulse duration. Clean ablation is only achieved in a narrow window from about 8ns to 12ns.

With further optimization of these parameters, excellent scribe quality was observed, but there remained a noticeable 'disc' marking of the glass by the laser which can be seen in Figure 4. Subsequent analysis revealed that this feature has no perceptible depth and there were no cracks or other overt defects left in the glass. We conclude that the "disc" marks the threshold at which there is a phase change in the Mo just before the onset of ablation. Furthermore the scribes showed excellent electrical isolation, beyond the limit of our measuring instruments. These optimized conditions, 250µJ 10ns square pulses (Figure 5), were later used to make the mini-modules.

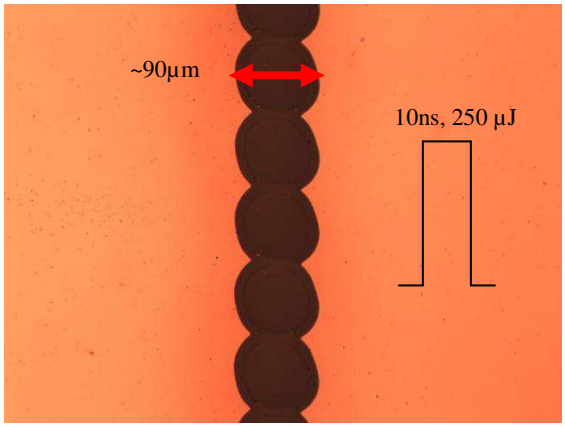

Figure 5: 200X optical image of optimized scribe process result. Maximum scribe width is about 90 µm. The ring in the center was found to have no significant depth and no cracks in the glass substrate were observed.

2.3 P2 Process

Unlike the P1 process, there have not yet been any commercial implementations of a laser scribe for the P2 or the P3 process. Those processes closest to being accepted by industry generally use picosecond pulses near 500nm wavelength [4]. However these processes still result in some melting of the CIGS and a significant reduction in shunt resistance which is detrimental, particularly on the P3 scribe. Figure 6 shows a typical P3 scribe made with a ps laser.

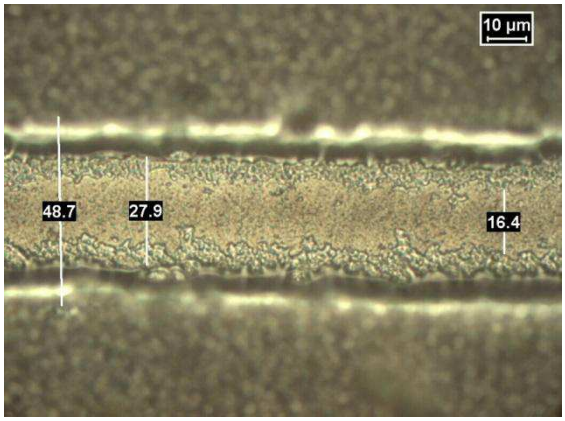

Figure 6: Typical P3 CIGS scribe with picosecond laser at 515 nm wavelength. *(Used with permission.)*

In contrast with the existing state-of-the-art laser scribe processes, the CIGS P2 process that was developed in this work results in no edge melting and very little residue in the bottom of the groove. Figure 7 below shows SEM images of a P2 scribe that was performed with the PyroFlex™-25 pulse programmable fiber laser. Note the complete absence of melt at the edges of the scribe and the clean bottom of the scribe.

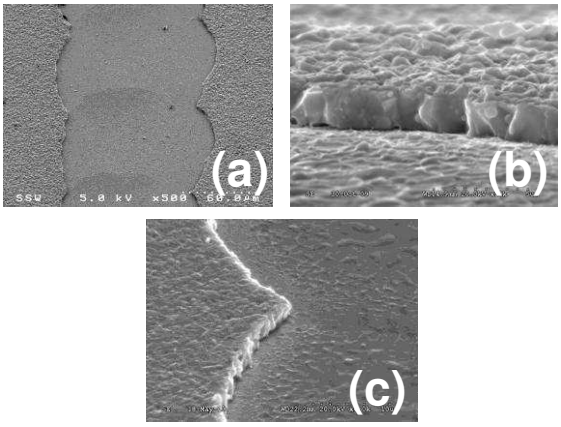

Figure 7: SEM images of edge quality for the PyroFlex CIGS P2 process. SEM images of PyroFlex CIGS P2 scribes (a) top view showing cleanliness of groove and fractured edges, (b) close up of fractured edge indicating no melting of the CIGS absorber layer, and(c) angle view of edge scallop between adjacent laser pulses.

In Figure 7 it is clear that there is some residue left at the bottom of the scribe. As seen in Figure 7(c), the surface texture in the trench bottom is suggestive of that which occurs when a mass of solid material is lifted from an underlying solid surface, with a fluid gel or viscous liquid film sandwiched between the two solid layers. This is suggestive of the underlying processes responsible for this ablation to be discussed later.

For the P2 scribe, the material that remains at the bottom of the groove is of particular interest since the top contact layer (typically Aluminum doped ZnO or AZO [8]) must make the contact to the bottom layer in this groove to make the cell-to-cell series interconnect. Any residue left in the groove could negatively affect the contact resistance and therefore the overall series resistance. With this in mind EDX scans (Figure 8) were performed with an emphasis on determining the composition of the residue at the bottom of the groove.

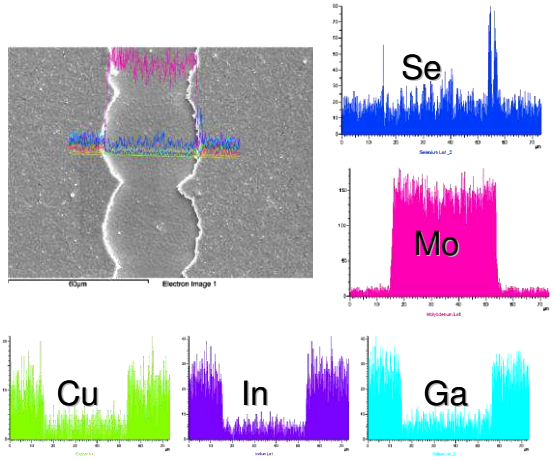

Figure 8: EDX analysis reveals excess selenium in the scribe trench and at the trench edges.

The EDX analysis reveals that the trench bottom contains only trace amounts of Cu, In, and Ga. The Se levels, however, are comparable to those on the surface of the bulk CIGS film. While this analysis gives a good indication that the residue in the trench is primarily selenium it does not indicate what the electrical properties of the material may be. As will be discussed later in the section on the modules created with these scribe processes, there does not appear to be any significant increase in series resistance for laser scribe grooves vs mechanically scribed grooves.

Also of interest is the process window over which the process behaves well in terms of pulse duration, pulse energy and focus depth. As part of this work we characterized these aspects of the process window thoroughly. We determined that nominal pulse duration was less than 5 ns and that both the rise and fall time of the pulse were critical parameters for achieving a robust result with a wide process window. The results of the pulse shape study are published in another work [9]. Figure 9 shows the process window in terms of pulse energy for a spot size of about 50 µm in diameter. The limit for a stable process runs from about 10 µJ to about 16 µJ which indicates a ± 25 % process window in energy. At lower energies the process simply fails to complete and at higher energies the amount of residue in the groove increases markedly and damage to the Mo layer in the form of pinholes and cracks appear.

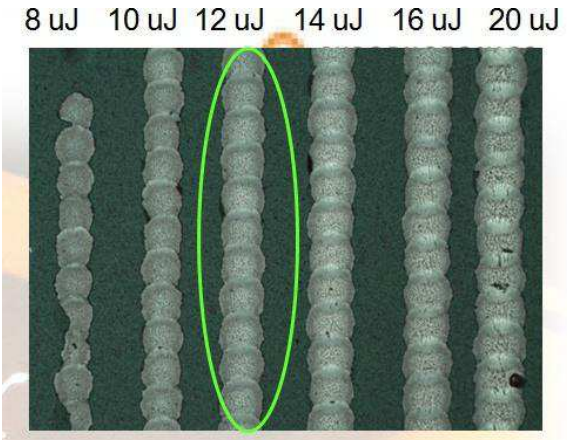

Figure 9: Robust process window with pulse energy. Robust process window extends from about 10 µJ to 16 µJ. Nominal scribe width is about 50µm, laser pulse rate = 20 kHz, and stage speed is 800 mm/s.

In addition to the energy process window, a key parameter that indicates that a process will be robust in an industrial environment is the depth of focus (DOF). To characterize the DOF we configure the laser system for the nominal energy of about 12 µJ and adjust the focus position of the delivery lens until the process begins to degrade noticeably in both the positive and negative z directions. Figure 10 shows the laser scribes as the focusing lens is adjusted in 0.2 mm steps through focus. As can be clearly seen the quality of the scribe lines is very good and effectively unchanged over an entire 2 mm range of motion of the delivery lens. This is a good indicator that the process can likely be robust over very large panels where the panel surface flatness may be an issue [10]. This DOF also speaks to the excellent M^2 value of the fiber laser, typically < 1.3. Furthermore the large DOF implies that a system design may not require autofocus optics for a robust process.

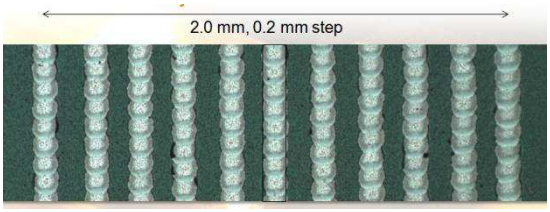

Figure 10: DOF of PyroFlex CIGS P2 process. Note that the process remains approximately unchanged over a ±1 mm focal depth with a 100 mm focal length delivery lens.

Finally the optimized scribing process was applied to the P2 step in fabrication of the mini-modules in collaboration with NREL. The picture in Figure 11 shows the resulting P2 scribe (right) next to the P1 scribe (left). More details with regard to the structure, fabrication and test of the resulting modules can be found in ref. [8, 11]. Also, it should be noted that the large scribe spacing (~210 µm) was chosen for consistency with typical mechanical scribing systems and is not limited by the laser process.

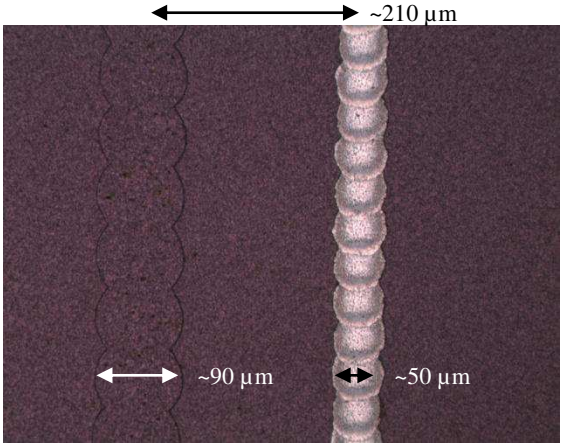

Figure 11: Sample of P2 scribe with optimized process as it was applied to the NREL mini modules. Note the ~90 um wide P1 scribe visible at left.

2.4 P3 Process

For the purposes of this work it was found that the scribing parameters for the P3 scribe were identical to the parameters for the P2 scribe. DOF, energy range, and pulse duration were all found to be approximately the same for both P2 and P3 so the data will not be repeated here. For P3, however, we also documented the process behavior as a function of the spot overlap. It was found that the process behaved well over a range of about 16 kHz to 24 kHz (10 – 40% spot overlap) with the process becoming less stable above 50% overlap. Figure 12 illustrates the scribe quality as a function of pulse overlap.

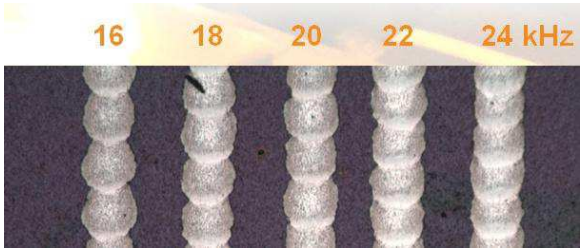

Figure 12: P3 scribe appearance as a function of laser spot overlap. Process is robust up to 24 kHz (~ 40% overlap) but begins to degrade at higher spot overlaps.

As with the P2 step, the P3 optimized scribe was applied to the mini-modules fabricated by NREL. After the P2 scribe was completed at PyroPhotonics, the modules were returned to NREL and the AZO top contact layer was applied. The modules were then returned to PyroPhtonics to apply the P3 scribe. This top contact layer is responsible for the bluish appearance of the P2 scribe as seen in Figure 13. The scribe spacing between the P2 and the P3 scribe is about 125 µm and again chosen to be comparable with existing mechanical scribe processes and is not limited by the laser process.

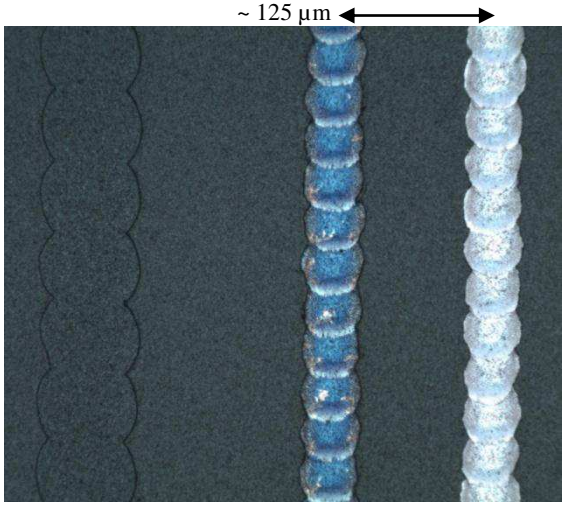

Figure 13: Sample of P3 (right) scribe as applied to the NREL mini-modules. Note the P1 scribe (left) and the P2 scribe (middle). The P2 scribe now has a bluish appearance due to the presence of the AZO layer that was applied at NREL between the P2 and the P3 steps.

2.5 P3 Rework, Edge Deletion and Defect Repair

After the P3 scribe, the same P3 process was used to perform edge deletion and to clear electrical contact pads so that the mini-modules could be tested. Initial test results however, indicated that the efficiency of the modules was only about 5% and that the series resistance was anomalously high. After investigation at NREL [8] it appeared that the initial AZO deposition had been too thin for the size of the cells in the mini-module. With this determination, the modules were returned to NREL after the P3 scribe for deposition of additional AZO material and then returned to PyroPhotonics for reworking the P3 step. Because it was critical to minimize the "dead zone" between the P1 and the P3 scribe, this time we placed the

new P3 scribe directly adjacent to the previous P3 scribe. As Figure 14 indicates, the spacing between the laser scribes can be made zero for all practical purposes and clearly demonstrates the potential of the laser process to reduce the dead space between the P1 and P3 scribe to near zero. After the additional AZO deposition and rework the module performance increased dramatically as discussed later.

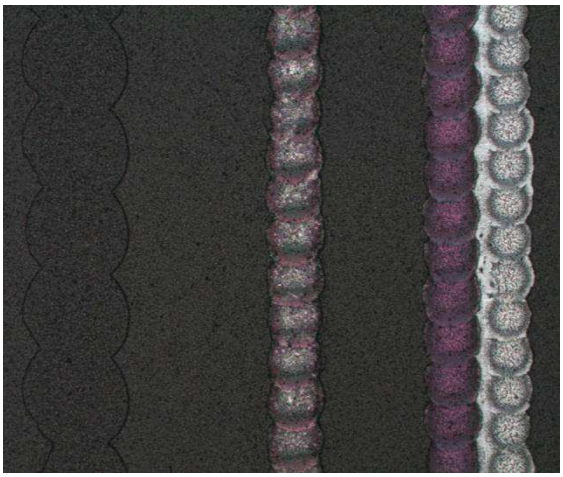

Figure 14: Far right, second P3 scribe added after the deposition of additional AZO material to the module. Note that the scribe spacing is effectively zero. Again the width of the P3 scribe is about 50 µm.

In addition to the P3 rework, the laser was used to delete the edges of the cells to ensure that there were no shorts between cells and that material non-uniformity near the edges did not negatively impact the performance of the modules. In addition several defects where the film was scratched in handling or otherwise damaged were identified. In places where these defects allowed shorting of the top and bottom conductor they were clearly detrimental to the performance of the cells and hence the entire module. Consequently the P3 process was used to isolate and/or remove these defects as shown in Figure 15. Similar processes were used to delete the material from the edges of the module and clear the electrical contacts so that the module could be tested.

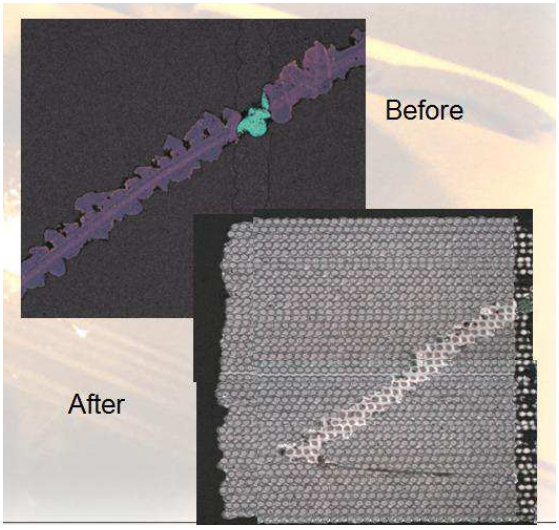

Figure 15: Example of how the laser was used to remove a shunting defect. Top: a scratch in the film before the AZO deposition resulted in a shunt between the front contact and the back contact on two cells. Bottom: many adjacent laser passes and a mask in the region of the defect are used to completely eliminate the defect. Defect area is approximately 1.5 mm square.

3 Mini-Module

3.1 Mini-Module Fabrication

As already described in the process development portion of this paper, the CIGS P1, P2 and P3 processes were applied to NREL material to create two fully functional mini-modules for testing. Details of the material structure and fabrication are found in the referenced works [8,11], and the process steps are outlined below:

a) Mo layer deposited on 75mm square glass substrates at NREL
b) P1 scribe applied at PyroPhotonics
c) Absorber layers applied at NREL
d) P2 scribe applied at PyroPhotonics
e) Top contact AZO layer applied at NREL
f) P3 scribe applied at PyroPhotonics, edges isolated, anode and cathode contacts cleared and simple electrical tests performed.
g) Module characterization at NREL and additional AZO deposition
h) P3 rework at PyroPhotonics.
i) Module characterization at NREL

As a control, a third sample was not laser scribed but was shipped between NREL and PyroPhotonics along with the scribed modules. That sample was later processed per NREL's standard cell processing procedure to serve as a reference.

In addition to the two laser scribed modules, two additional modules were fabricated. However, this second pair of modules was sent to Jenoptik for the P2 and P3 scribes that were applied using a stylus scribing system. Other than the fact that these materials were mechanically scribed for P2 and P3, they were identical to the laser scribed modules. Figure 16 gives an overview of the physical series interconnect structure that

was formed by the P1, P2 and P3 scribes, depicts how successive P3 scribes at each edge of the module were used to created the anode and cathode contacts, and lastly shows the physical appearance of the all laser scribed functional mini-modules.

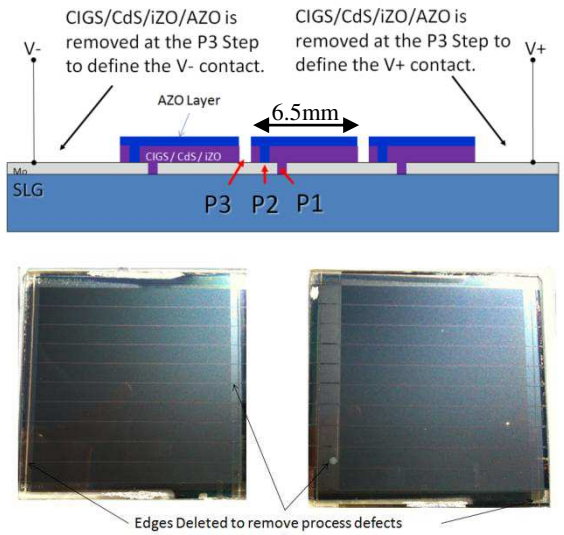

Figure 16: (Top) Electrical / Mechanical structure of mini-module cell interconnects. The cathode and anode contacts were formed by using the PyroFlex P3 process with hundreds of successive scribes placed adjacent to one another. (Bottom) Appearance of actual mini-modules after all laser processing, including edge deletion and defect deletion.

3.2 Mini-Module Test

Once the mini-modules were fabricated they were tested in direct sunlight by PyroPhotonics. In order to estimate the solar flux a laser power meter was pointed toward the sun and the power reading was divided by the absorber surface area in order to calculate the solar flux. To characterize the module performance both open circuit voltage (Voc) and short circuit current (Isc) were measured. Next, various load resisters were applied to each module and the cell efficiency was calculated as the power dissipated in the load resistor divided by the estimated solar flux on the module. The initial measurement taken after the first AZO deposition and first P3 scribe indicated that the maximum module efficiency was only about 5%, results that were later confirmed at NREL. With some investigation we suspected that the AZO layer was too thin for the chosen width of each cell in the module (6.5 mm). This resulted in an excessively high series resistance and larger internal power loss in the module. Additional AZO was added by NREL, and the modules were then P3 scribed a second time (Figure 14). Again the modules were tested at PyroPhotonics and at NREL. The initial testing at PyroPhotonics indicated about a factor of two improvement in the module efficiency as shown in Figure 17(top). Figure 17 (bottom) shows the result of subsequent testing at NREL under standard test conditions (STC). The difference between the two results is attributable to the non-standard illumination conditions used at PyroPhotonics, but they are generally consistent.

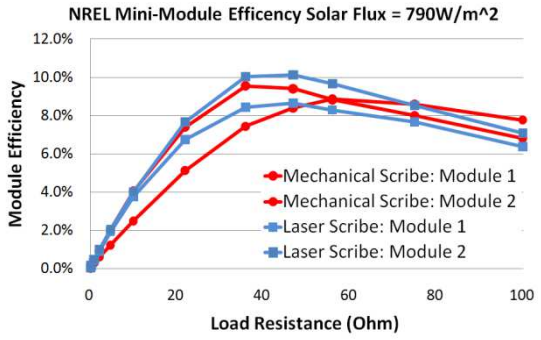

Mini-Module Meas. ID	Total AZO (µm)	Voc (V)	Jsc (mA/cm^2)	FF (%)	Eff. (%)	Rs (ohm-cm)	Rsh (ohm-cm)	Scribing Method
C2681-1	0.12	5.742	26.97	34.30	5.31	113.6	503.4	All Laser
C2681-2	0.50	5.846	26.74	46.32	7.24	81.9	697.2	10 cells
C2684-1	0.12	4.979	27.61	29.65	4.08	128.0	280.5	All Laser
C2684-2	0.50	5.975	26.76	51.93	8.30	48.1	726.0	10 cells
C2682-2	0.50	5.811	25.16	51.18	7.48	49.2	999.8	Laser + Mechanical 10 cells
C2683-2	0.50	5.458	25.19	48.22	6.63	50.3	761.1	Laser + Mechanical only 9 cells

Figure 17: (Top) Laser scribed and mechanically scribed mini-module efficiency as a function of load resistance under 790 W/m^2 estimated solar flux. (Bottom) I-V parameters as measured at NREL under Standard Test Conditions (STC).

As Figure 17(top) clearly indicates, the efficiencies of the laser scribed modules and the mechanically scribed modules are comparable. The best module, just over 10% (8.3% NREL STC) efficiency, is a laser scribed module where as the second best module at about 9.8% (7.5% NREL STC) is one of the mechanically scribed modules. The control sample that was processed with NRELs standard process indicated that the material was capable of reaching 16% (STC) efficiency [8], suggesting that there were some deficiencies in the mini-module structures that limited the performance. The fact that there are no systematic differences in performance between the laser scribed modules and the mechanically scribed modules implies that laser scribing results in no sacrifice in performance compared with mechanical scribing. NREL is currently characterizing these modules further to determine what issues are limiting the performance of these modules [8].

3.3 Mini-Module Conclusions

With the results from the mini-modules we conclude that the laser P2 and P3 scribe processes produce modules that are of at least equal performance to a mechanical P2 and P3 scribes if not better. We also note that there is no intrinsic limit to the spacing of the laser scribes and that they can be placed directly adjacent to one another, being limited only by the process of mechanical registration. This ability to place the scribes very close together should allow reduction of the resulting "dead space" between the P1 and P3 scribe that in turn should allow reduction of the overall "dead zone" and a concomitant increase in efficiency.

4 Ablation Process Physics

In another published work we advance a phenomenological model that describes the physical processes underlying this novel ablation process [11]. Here, we briefly recap our conceptual model for this "brittle fracture" process with some modifications that

reflect some further insight we have gained through some simple numerical modeling.

4.1 Physical Process Overview

We have summarized our understanding of the mechanisms underpinning this ablation process as a competition between two processes, one that drives the brittle fracture process to completion and another that spoils the brittle fracture process. These two mechanistic paths are proposed in Figure 18.

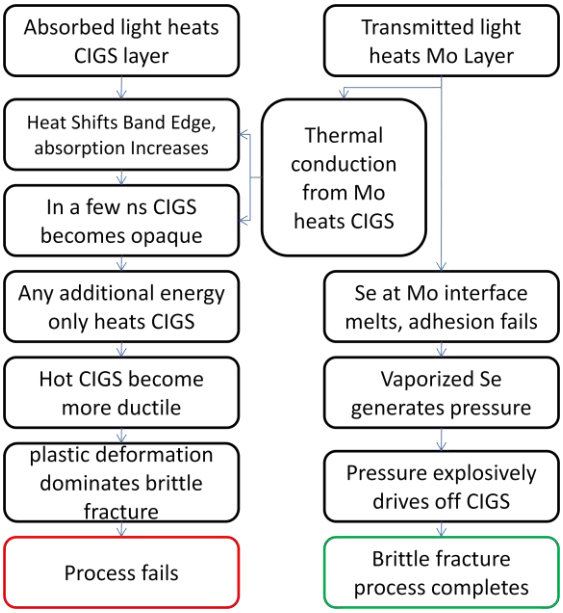

Figure 18: Conceptualization of two competing processes proposed for the laser-material interaction. The process in the left column moves toward spoiling the brittle fracture ablation process where as the one on the right tends toward completing the brittle fracture process.

Referring to Figure 18 we can make the following generalizations about the process:

1. Thermal conduction from the Mo into the CIGS puts an upper time limitation on the duration of the laser pulse.
2. Slow rise time on the laser pulse will limit the total peak energy that can reach the Mo layer, meaning that the CIGS gets too hot and becomes mechanically plastic before the Se vapor pressure reaches a level that can drive an ablation process
3. A long fall time for the pulse will only contribute additional heating to the CIGS layer and spoil the brittle fracture process which we believe evolves over a period of several nanoseconds.
4. Excess peak power causes non-linear optical absorption in the CIGS.

As mentioned at the beginning of this paper, until now there has been no report of successful CIGS P2 and P3 scribing utilizing a nanosecond class 1064 nm pulse laser. Furthermore, the process parameters that were found to be appropriate for this work have since proven to be also appropriate for nearly a dozen different P2 and P3 material samples from many different suppliers. This then begs the question of why this process has not already been reported in the literature and why the PyroFlex™-25 pulse programmable fiber laser is uniquely capable of consistently generating this ablation phenomenon over a relatively wide range of process conditions. We postulate that the answer lies in examination of the points listed above.

To examine the first point we constructed a very simple thermal diffusion model using real CIGS thermal properties to determine the time scale on which thermal diffusion became important. There are a number of ways that such a thermal diffusion problem can be modeled [12,13], however we chose to model the CIGS as a cylinder with a heat source inside (Figure 19 top). The resulting 1-D thermal diffusion model quite interestingly predicted that the time constant for thermal diffusion from the Mo into the CIGS is about 5 ns (Figure 19), consistent with our observation that the process begins to fail at pulse durations longer than about 5 ns.

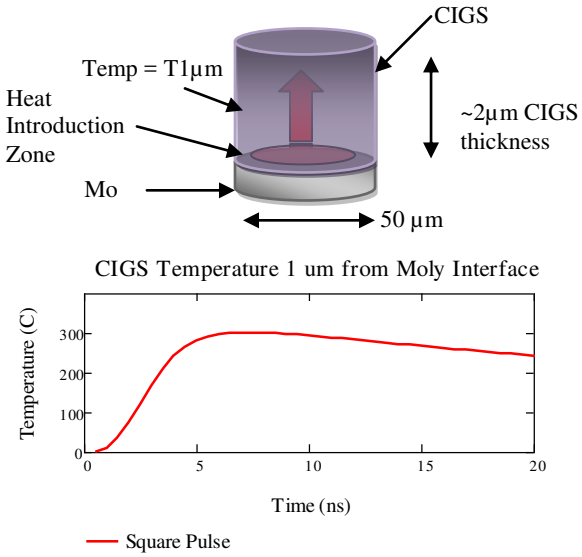

Figure 19: One dimensional thermal diffusion model. (Top) Heat is deposited at the Mo-CIGS interface by the laser pulse and diffuses upward. (Bottom) Plot showing the solution as a function of time for the 1-D diffusion equation at the mid plane between the Mo layer and the top surface (T1µm).

To examine the second point we also constructed a very simple linear absorption model and simulated the expected transmission of the laser pulse to the Mo layer. The results of this simple modeling exercise are shown in Figure 20 and show the peak intensity of the laser pulse that develops at the Mo layer for a pulse of fast rise time and a pulse of comparatively low rise time. The plot clearly shows that a pulse of slower rise time results in proportionally lower peak intensity on the Mo layer than would be predicted just based on the relative peak intensity of the starting pulses. This can simply be understood as the fact that heating due to the leading edge increases the CIGS absorption coefficient before the peak of the pulse can arrive. In our laboratory experiments we do indeed find that increasing the rise time has a negative impact on the ablation process and narrows the process window in energy.

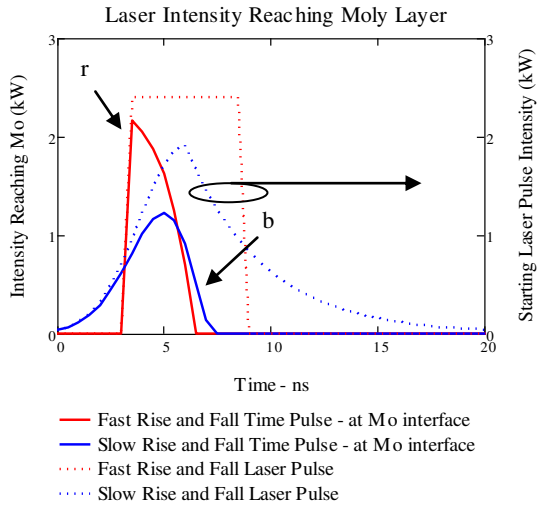

Figure 20: Solid Curves: Laser pulse intensity reaching the Mo surface for two different pulses. Dotted Curves: (r), a 5ns duration rectangular pulse (fast rise and fall time); (b), a 5ns FWHM Q-switched pulse (slow rise and fall time). Both shapes contain equal pulse energy but due to the long rise time on (b) the peak intensity reaching the Mo interface is proportionally lower.

To address the third point, how pulse fall time affects the brittle fracture ablation process, we consider the evolution in time of the mechanical properties of the CIGS film. The brittle fracture process has been so described because the film is literally blown off of the Mo surface while still in the solid state. The edges left behind are mechanically broken and completely free of melt. Thermal conduction from the Mo layer into the CIGS layer, and/or the absorption of additional energy within the CIGS layer after it has reached opacity, heats it further. As CIGS approaches its melting point there will be a transition from brittle ceramic-like behavior to a more ductile-type behavior. Referring to Figure 21, in general the energy required to fracture can be considered as proportional to the area under the stress-strain curve for the material [14]. Figure 21 shows how an idealized stress strain curve may look for a brittle material when it is cold (blue) and when it is hot (red). From the figure it is clear that the material at higher temperature will absorb much more energy before finally undergoing fracture (red "x" in the figure) than the cooler material. Consequently if the material is allowed to become too hot, the energy being released by the explosive expansion of selenium at the Mo interface is consumed in the plastic deformation of the material rather than fracture and ejection of the debris. The end result is melted mass of CIGS rather than clean, brittle material ejection.

Figure 22 depicts the process window in terms of DOF, for a pulse of 8 µJ, for pulses with a) short rise and fall time, b) long rise time, and c)long fall time. As our model predicts rise and fall time appear to be critical parameters to establish a robust process window.

Finally, we address our fourth point. Given that ours is the first work in the field to address these problems with a pulse-shaped laser, we conclude that the only previous work to have utilized short rise time and short fall-time pulses have involved picosecond lasers. According to our arguments above, these should have been sufficient to drive the brittle fracture process. However, they have not done so, and appear only to have succeeded in producing a regular vaporization-based ablation mechanism with melted CIGS at the side walls. We therefore postulate the following factors that have prevented ps lasers from achieving the brittle fracture result:

1. Increased non-linear absorption results in a larger fraction of energy absorption in the CIGS rather than Mo layer.
2. Pulse energies are too low.
3. PRF is too high in mode locked systems to allow single pulse delivery.
4. CW background levels are too high. (From our own work we have determined that any CW background also spoils the process.)

In several references examined [15,16,17], we see that at least one or more of the above points is at work and would have prevented the success of the brittle fracture mechanism. Most relevant is the potential increase in absorption in the CIGS layer due to non-linear effects caused by high peak power. This mandates that the ideal pulse delivers the certain net energy required within a pulse being substantially shorter than 5ns, with fast rise and fall times, and with a limitation of the peak power. These conditions require an essentially square pulse shape.

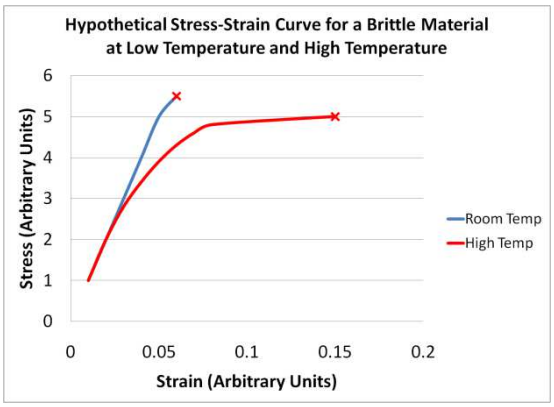

Figure 21: Hypothetical stress strain curve for a material at two different temperatures. The red "x" represents the breaking stress.

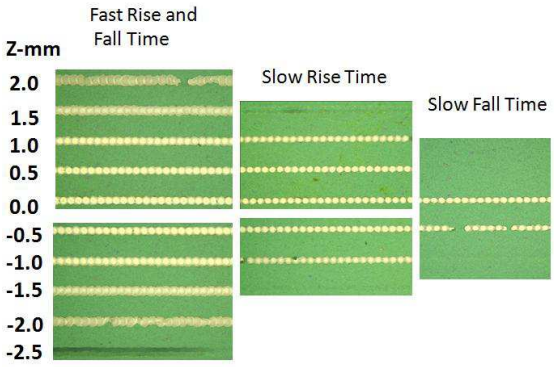

Figure 22: Impact of laser pulse rise and fall time on process window with pulse energy = to 8 µJ. Z-mm (vertical axis) represents the process DOF in mm.

4.5 Process window and the laser pulse

While this is by no means a complete or rigorous analysis of the mechanisms at work in this ablation process, the correlation of physical results and the trends that our model predicts indicate that this model provides a good starting point for understanding of this ablation process. It also gives an indication of why existing lasers have not been able to exploit this ablation mechanism for CIGS as the PyroFlex™-25 has. Namely, Q-switched lasers and fiber lasers available until now have not provided the combination of fast rise time, fast fall time, short overall pulse duration and sufficient energy content per pulse that is required to drive this process forward at 1064 nm.

In terms of establishing a robust manufacturing process we have established that the pulse properties of pulse programmable fiber laser allow the laser to operate comfortably inside of this ablation process window. The resulting process for P2 and P3 have excellent DOF, comfortable tolerance for energy fluctuations, and the PyroFlex™-25 has sufficient pulse energy available so that many scribes can be made in parallel. We find the added advantage that the exact same laser can be used also for the P1 scribe with the same optical configuration. This opens the door to a single process machine for all three P1, P2, and P3 processes. Even edge isolation and repair of large defects are possibilities.

5 Summary

We have outlined the development of CIGS P1, P2, and P3 scribe processes with the PyroFlex™-25 pulse programmable fiber laser. The P1 process developed was found to be comparable to other commercial P1 processes with excellent groove quality. The P2 and P3 processes were found to remove the CIGS material in a “brittle fracture” manner with no melting and little residue left in the trench bottom. The process window was found to be broad in terms of DOF and pulse energy and 5ns was established as an upper limit on pulse duration for establishing the best process. The processes developed were put to work in cooperation with NREL to fabricate mini-modules to test the viability of this all-laser scribing process for the production of monolithic series interconnected solar modules. For comparison mini-modules were also fabricated utilizing mechanical scribing for the P2 and P3 steps. The resulting performance of the laser scribed and mechanically scribed cells was found to be comparable, leading to the conclusion that the laser scribe process is capable of similar if not better performance than the mechanically scribed process. More work and study shall enable us to fine-tune the scribing conditions and to improve the performance of mini-modules. Finally we put forward a model for the ablation mechanism that involves a competition between the desired brittle fracture ablation process and a competing parasitic process. We offered a qualitative interpretation of some modeled and some empirical data that give a framework for understanding which pulse parameters are important for favoring the “brittle fracture” process over the parasitic process. This interpretation also gives insight as to how the pulse characteristic of the PyroFlex™-25 pulse programmable fiber laser allow it to operate in this “brittle fracture” process window where as other lasers to date have failed.

ACKNOWLEDGEMENT

The authors would like to acknowledge the contribution of JENOPTIK Automatisierungstechnik GmbH to this paper, and in particular to thank Dr Gabriele Eberhardt and Dr Torsten Reichl for their support.

References

[1.] **Q-Cells SE.** Q-Cells sets a new 13.0 % efficiency record for mass-produced CIGS thin-film modules . *Q.cells.* [Online] June 9, 2010. [Cited: July 21, 2010.] http://www.q-cells.com/en/company/press/corporate_news/index.html.

[2.] **Claudia Brusdeylins.** Press Releases. *Zentrum für Sonnenenergieund und Wasserstoff-Forschung Baden-Württemberg (ZSW).* [Online] April 28th , 2010. [Cited: July 21, 2010.] http://www.zsw-bw.de/fileadmin/ZSW_files/Infoportal/Presseinformation en/docs/pi05-2010-ZSW-Worldrecord-TF-CIGS.pdf.

[3.] **Jha, A. R.** *Solar Cell Technology and Applications.* Boca Raton : Auerbach Publications, 2009. p. 21.

[4.] *Structuring of thin film solar cells.* **Eberhardt, Gabriele, et al.** San Jose : SPIE, 2010. Proceedings Vol. 7585.

[5.] **Murison, Richard, et al.** *7,742,511* USA, 2008.

[6.] *Thin film removal mechanisms in ns-laser processing of photovoltaic materials.* **Bovatsek, J.** s.l. : Thin Solid Films, 2010. Vol. 518, pp. 2897-2904.

[7.] *Large-Area CIGS Modules: Processes and Properties.* **Powalla, M., Hariskos, D. and Lotter, E et al.** s.l. : Thin Solid Films, 2003. 523-533.

[8.] *ALL-LASER SCRIBING FOR THIN-FILM CuInGaSe2 SOLAR CELLS.* **F.J. Pern, et al.** s.l. : IEEE, 2010. IEEE PVSC.

[9.] *Application of a pulse programmable fiber laser to a broad range of Micro-Processing Applications.* **Rekow, Mathew and R., Murison.** Anaheim : LIA, 2010.

[10.] **Patel, Rajesh and Bovatsek, James.** Why M2 matters. *http://www.optoiq.com/.* [Online] May 2010.

[11.] *CIGS P1, P2, AND P3 LASER SCRIBING WITH AN INNOVATIVE FIBER LASER.* **Richard Murison, et al.** s.l. : IEEE, 2010. IEEE PVSC.

[12.] **Elżanowski, Marek.** http://www.mth.pdx.edu/~marek/mth510pde/notes%202.pdf. *http://www.mth.pdx.edu.* [Online]

[13.] *Laser Flash Method for Estimating the Thermal Diffusivities of Thin Films.* **Peichun, YANG, Hou, Li and Lichang, Qi.** Beijing : KTK Scientific Publishers, 1990.

[14.] *The effect of strain rate on the stress–strain curve of oriented polymers. .* **Hall, I. H.** 4, s.l. : Journal of Applied Polymer Science, 1968, Vol. 12.

[15.] *Picosecond-Laser Structuring of Thin Films for CIGS Solar Cells.* **Gediminas, Račiukaitis and Paulius, Gečys.** Vilnius : LAMP2009, 2009.

[16.] *ps-laser scribing of CIGS films at different wavelengths.* **Gečys, P., et al.** Berlin / Heidelberg : Springer, 2010-06-18. 0947-8396.

[17.] **Compaan, Alvin.** photovoltaics-laser-scribing-creates-monolithic-thin-film-arrays.html. *http://www.optoiq.com/.* [Online] Jan 01, 2000. [Cited: 9 2, 2010.]